Ca^{2+} Release from the Sarcoplasmic Reticulum Compared in Amphibian and Mammalian Skeletal Muscle

NATALIA SHIROKOVA, JESÚS GARCÍA, GONZALO PIZARRO, and EDUARDO RÍOS

From the Department of Molecular Biophysics and Physiology, Rush University School of Medicine, Chicago, Illinois 60612

ABSTRACT Puzzled by recent reports of differences in specific ligand binding to muscle Ca^{2+} channels, we quantitatively compared the flux of Ca^{2+} release from the sarcoplasmic reticulum (SR) in skeletal muscle fibers of an amphibian (frog) and a mammal (rat), voltage clamped in a double Vaseline gap chamber. The determinations of release flux were carried out by the "removal" method and by measuring the rate of Ca^{2+} binding to dyes in large excess over other Ca^{2+} buffers. To have a more meaningful comparison, the effects of stretching the fibers, of rapid changes in temperature, and of changes in the Ca^{2+} content of the SR were studied in both species. In both frogs and rats, the release flux had an early peak followed by fast relaxation to a lower sustained release. The peak and steady values of release flux, R_p and R_s, were influenced little by stretching. R_p in frogs was 31 mM/s (SEM = 4, n = 24) and in rats 7 ± 2 mM/s (n = 12). R_s was 9 ± 1 and 3 ± 0.7 mM/s in frogs and rats, respectively. Transverse (T) tubule area, estimated from capacitance measurements and normalized to fiber volume, was greater in rats (0.61 ± 0.04 μm^{-1}) than in frogs (0.48 ± 0.04 μm^{-1}), as expected from the greater density of T tubuli. Total Ca in the SR was estimated as 3.4 ± 0.6 and 1.9 ± 0.3 mmol/liter myoplasmic water in frogs and rats. With the above figures, the steady release flux per unit area of T tubule was found to be fourfold greater in the frog, and the steady permeability of the junctional SR was about threefold greater. The ratio R_p/R_s was ~2 in rats at all voltages, whereas it was greater and steeply voltage dependent in frogs, going through a maximum of 6 at −40 mV, then decaying to ~3.5 at high voltage. Both R_p and R_s depended strongly on the temperature, but their ratio, and its voltage dependence, did not. Assuming that the peak of Ca^{2+} release is contributed by release channels not in contact with voltage sensors, or not under their direct control, the greater ratio in frogs may correspond to the relative excess of Ca^{2+} release channels over voltage sensors apparent in binding measurements. From the marked differences in voltage dependence of the ratio, as well as consideration of Ca^{2+}-induced release models, we derive indications of fundamental differences in control mechanisms between mammalian and amphibian muscle.

INTRODUCTION

The flux of Ca^{2+} release from the sarcoplasmic reticulum, measured in skeletal muscle fibers under voltage clamp, includes two well-defined kinetic components, a fast early peak and a maintained phase of release (Baylor et al., 1983; Melzer et al., 1984, 1987). It has been proposed that these components reflect release through two different sets of channels (Ríos and Pizarro, 1988), one activated by Ca^{2+} and the other directly by voltage. This proposal is consistent with experimental results of Jacquemond et al. (1991) using intracellular Ca^{2+} buffers, and the "skipping" pairing of release channels with T membrane tetrads (putative DHP receptors/voltage sensors) found in the triadic junction of fish (Block et al., 1988) and peripheral couplings of embryonic mouse, frog slow, and cultured human muscle (Franzini-Armstrong and Kish, 1995). In this proposal, release channels not paired with tetrads are Ca^{2+} operated and contribute the peak component of release, whereas those paired with DHP receptors/

Address correspondence to Dr. E. Ríos, Department of Molecular Biophysics and Physiology, Rush University School of Medicine, 1750 West Harrison Street, Chicago, IL 60612.

Dr. Shirokova's permanent address is A. A. Bogomoletz Institute of Physiology, Ukrainian National Academy of Sciences, Bogomoletz St.4, 252601 GSP, Kiev 24, Ukraine.

Dr. García's current address is Department of Physiology, Colorado State University, Fort Collins, CO 80523.

Dr. Pizarro's permanent address is Departamento de Biofísica, Facultad de Medicina, Montevideo, Uruguay.

J. GEN. PHYSIOL. © The Rockefeller University Press • 0022-1295/96/01/1/18 $2.00
Volume 107 January 1996 1–18

voltage sensors are directly controlled by voltage and contribute the steady component.

In this context, an interesting structural difference between skeletal muscle fibers of amphibians and mammals has recently been revealed. In measurements of specific DHP and ryanodine binding in frog muscle, ratios of ryanodine to DHP receptors are consistently higher than in mammalian muscle (Anderson et al., 1990; Lamb, 1992; Bers and Stiffel, 1993; Margreth et al., 1993; Anderson et al., 1994). Just on this basis, the dual control model predicts a greater contribution of Ca^{2+}-induced release in amphibians, and a consequently greater peak component of release flux.

The differences between amphibian and mammalian release channels appear to be qualitative as well. Two isoforms of release channels are present in amphibian and avian muscle (Airey et al., 1990; Lai et al., 1992; Murayama and Ogawa, 1992; O'Brien et al., 1993) in about equal numbers (Conti et al., 1995). These two isoforms are also detected in mammalian muscle, but RyR1, the "skeletal" isoform, is much more abundant (Conti et al., 1995). The corresponding avian isoform, named α, has been implicated in the characteristic skeletal E-C coupling mechanism through studies of the crooked neck dwarf mutation (McKemy et al., 1995), whereas the β isoform has been shown to support cardiac-style E-C coupling, strictly dependent on external Ca^{2+}, and presumably involving Ca^{2+}-induced release mechanisms (McKemy et al., 1995). On this basis one would expect qualitative differences in the physiology, with a greater involvement of Ca^{2+}-dependent mechanisms in the nonmammalian muscle, and, again, a greater peak in the release waveform.

In the present work, we took advantage of recently described techniques (García and Stefani, 1990; Delbono and Stefani, 1993; García and Schneider, 1993) and quantitatively compared release flux in skeletal muscle fibers of the frog and the rat, under experimental conditions as uniform as possible, with special emphasis on quantification of the two kinetic components of release flux and their ratios. To make the comparison meaningful, we had to explore the effects of stretching, temperature, and SR loading on the quantitative aspects of release flux.

METHODS

Experiments were carried out in cut segments of fast twitch fibers from the m. semitendinosus of the frog (*Rana pipiens*) and the extensor digitorum longus of the rat (*Rattus norvegicus*, Sprague-Dawley), voltage clamped in a double Vaseline gap. The fiber preparation procedures and the design of the chamber and voltage clamp were as described in detail, for frog muscle, by Kovács et al. (1983); Brum et al. (1988); Francini and Stefani (1989); and González and Ríos (1993). The adaptation of the technique for rat muscle was as described by García and Schneider (1993) and Delbono and Stefani (1993). The membrane in the end pools was permeabilized by saponin (Irving et al., 1987).

$[Ca^{2+}]$ and its changes were monitored with two optical methods, singly or in combination. One was the use of absorption signals from antipyrylazo III (ApIII), a technique described in detail by Brum et al. (1988). The other was the use of fluorescence signals from the dyes fluo-3 or calcium green-1. These dyes have some advantages over fura-2, including excitation and emission at visible wavelengths and relatively high reaction rates, given their high affinity.

In most cases both measurements were carried out simultaneously, using a multiwavelength microscope arrangement, inspired by one described by Klein et al. (1988) for the simultaneous use of ApIII and fura-2 and represented in Fig. 1. All filters and dichroic mirrors used in the setup were custom made by Omega Optical, Inc. (Brattleboro, VT). Light from a 100-W tungsten-halogen bulb (*LA*) was used in Köhler illumination mode to pass a beam of light of adjustable dimensions through the fiber. This beam contained wavelengths longer than 600 nm (filter *IFA*) that were used to elicit absorption signals from ApIII and intrinsic absorption signals as described by Brum et al. (1988). A second halogen lamp (*LF*) was used to excite fluorescence in epi-illumination mode. An interference filter (*IFE*; 490 nm, 10-nm bandwidth) trimmed the excitation beam, which was reflected into the microscope objective (*IO*; 40×, water immersion) (Zeiss 561702; Carl Zeiss, Inc., Thornwood, NJ) by a 510-nm high pass dichroic mirror (*DM1*). The emitted light of longer wavelength and all the transmitted light passed through this mirror. A second dichroic (*DM2*) reflected light of <550 nm (containing most of the fluorescence emission), which was then filtered at 530 nm (by interference filter *IF1*) and focused on a photodiode connected in photoresistive mode (*PD1*) (model HUV-200; EG & G Canada, Vaudreuil Quebec, Canada). Light $\lambda > 550$ nm was split by DM3, which reflected $\lambda < 800$ nm. The reflected light was filtered at 720 nm (*IF2*) and detected by photodiode PD2; it contained the Ca^{2+}-dependent signal of the absorption dye. The light transmitted through DM3 was filtered at 850 nm (*IF3*) and detected by PD3, it contained the intrinsic, dye-independent signal.

The intensities at 720 and 850 nm were conditioned by track-and-hold subtraction (Brum et al., 1988); the fluorescence intensity (at 530 nm) was simply amplified. All signals were filtered at half the frequency of final storage with 8-pole Bessel filters of adjustable frequency (7951T-8; Frequency Devices, Inc., Haverhill, MA). All three intensities were acquired, simultaneously with membrane voltage and current, at a collective rate of 100 kHz with 16-bit nominal resolution (HS-DAS 16; Analogic Corp., Peabody, MA). Therefore, the rate per individual channel was 20 kHz. The signals were decimated by averaging and stored at 125 ms per point or lower frequency if desired.

Ca^{2+} Release from Absorption Dye Signals

After Ca^{2+} transients (time course of the change in intracellular $[Ca^{2+}]$) were obtained by conventional methods, the method of Melzer et al. (1984) was used to derive release flux. In this method, release flux is determined as the sum of the removal flux plus the time derivative of the free $[Ca^{2+}]$. The removal flux is determined empirically from the decay of the $[Ca^{2+}]$ transient after depolarizing pulses, and the description is parametrized by fitting a removal model. When using a high concentration of EGTA inside the cells, the time course of the free $[Ca^{2+}]$ is close

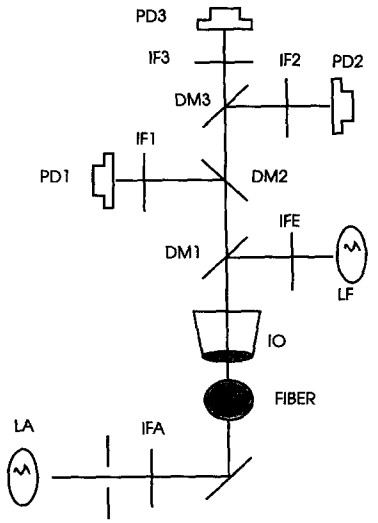

FIGURE 1. Device for monitoring Ca^{2+} with absorption and fluorescent dyes. The fiber was voltage clamped in a Vaseline gap chamber located in the cooled moving stage of a modified upright microscope. It was illuminated simultaneously with long wavelength light for absorption measurements, coming through an inverted objective under the fiber, and short wavelength light for fluorescence excitation. The sources for both were tungsten-halogen bulbs (*LA* and *LF*). Different wavelengths were separated by dichroic mirrors (*DM1, 2,* and *3*) and defined by interference filters (*IFE, IF1, 2* and *3*). The three photodiodes (*PD1, 2* and *3*) measured respectively, fluorescent emission, the absorption dye signal at 720 nm, and intrinsic absorption changes of the fiber at 850 nm. Details of wavelength separation and filtration are given in the text.

to proportional to the release flux (Ríos and Pizarro, 1991; González and Ríos, 1993).

Ca^{2+} Release from Fluorescent Dye Signals

The use of fluo-3 and calcium green-1 simplifies the determination of release flux and avoids methodologic artifacts. Given their high affinity and relatively fast rates of Ca^{2+} binding, these dyes become the dominant agents of Ca^{2+} removal when they are present inside the cell at concentrations of 500 μM or greater. In these cases, they provide a simple minimum estimate of Ca^{2+} release as the rate of change of dye-bound Ca^{2+}, which in turn is proportional to the change in fluorescence. Therefore, when the fluorescent dyes were present at high concentrations, this approximation could be used without need for an estimate of the free $[Ca^{2+}]$ associated with the signal. In many cases, however, it was better to use the time derivative of the fluorescent-dye–bound Ca^{2+} as a "floor" and add to it other (minor) contributions to Ca^{2+} release, namely, the time derivative of the free $[Ca^{2+}]$ and the intrinsic removal fluxes. To do this, it was necessary to derive $[Ca^{2+}](t)$ from the dye signal and then apply the conventional removal method.

Ca^{2+} Transients from Fluorescent Dye Signals

On binding Ca^{2+}, calcium green-1 and fluo-3 simply scale their fluorescence by a factor greater than 1. The increase in fluorescence is therefore proportional to the concentration of Ca^{2+}-bound dye. In the low concentration limit, the proportionality factor is proportional to the dye concentration and to the fiber volume in the illuminated region. In the experiments described here, where high dye concentrations were used, autofiltration effects were major and taken into account. The practical relationships used to derive $[Ca^{2+}](t)$ from the fluorescence intensity $F(t)$ are given below and demonstrated in Appendix A.

Let F_{min} and F_{max} be the fluorescence intensities at zero and saturating $[Ca^{2+}]$. The fraction of dye bound to Ca^{2+} is $(F - F_{min})/(F_{max} - F_{min})$. In the equilibrium situation

$$[Ca^{2+}] = \frac{K_D (F - F_{min})}{F_{max} - F}, \tag{1}$$

F_{min} is given by

$$F_b + 0.75 q_{min} I_0 \frac{\epsilon_{490}}{\epsilon_{490+530}} \{1 - \exp[-\ln 10 \; D_1 (\epsilon_{490} + \epsilon_{530}) p]\} d, \tag{2}$$

where F_b is background fluorescence, q_{min} depends on the quantum efficiency of fluorescence and geometry of illumination and light collection, I_0 is the incident light intensity, ϵ_λ are the extinction coefficients of the fluorescent dye, D_1 is dye concentration, p (path) and d (diameter) are dimensions of the fiber along the illumination axis and perpendicular to it and to the longitudinal axis, respectively, and 0.75 is a correction factor for an elliptic rather than rectangular section of the fiber. F_{max} is calculated with Eq. 2, replacing q_{min} by q_{max}. Eq. 2 is an approximation; the more accurate Eq. A6 was used in practice (see Appendix A).

Parameter values were obtained from calibrations, carried out inside capillaries of various diameters, in the microscope setup. q_{min} was obtained with solutions of known dye concentration and nominally 0 $[Ca^{2+}]$. q_{max} was measured using the same solutions with excess Ca^{2+}. The measured ratio q_{max}/q_{min} was 63.75 for lot 2641 of fluo-3 and 12.2 for lot 2221 of calcium green-1. K_D in cuvette calibrations was 0.460 μM for fluo-3 and 0.188 μM for calcium green-1 (these values are changed, as explained later, based on kinetic comparisons inside fibers). The dye concentration was determined by measuring the absorbance of the fiber at 510 nm, near an isosbestic wavelength for fluo-3 (Harkins et al., 1993). The extinction coefficients for fluo-3 at 490, 510, 530, and 550 nm were measured in capillaries as 3.80, 3.98, 0.95, and 0.15 × 10^4 $M^{-1}cm^{-1}$, respectively. The corresponding values for calcium green-1 were 2.97, 6.35, 1.22, and 0.07, while for ApIII they were 1.22, 1.81, 2.20, and 2.44 * 10^4 $M^{-1}s^{-1}$.

Both fluorescent dyes used are slower than ApIII, and their equilibration lags substantially behind the experimental Ca^{2+} transients. The time course $[Ca^{2+}](t)$ was calculated from the dye signal as

$$\frac{k_{ON}^{-1}\frac{dF}{dt} + K_D (F - F_{min})}{F_{max} - F}. \tag{3}$$

This kinetic calculation required an estimate of the kinetic constants of the dye in the cytoplasm. This was carried out in the experiments by having at the same time one fluorescent dye and ApIII, assuming the rate constants for ApIII to be equal to their cuvette values and adjusting the kinetic constants of the fluorescent dye for the Ca^{2+} transients derived from both dyes to be as close as possible. Fig. 2 *A* shows the signals of absorption and flu-

orescence obtained simultaneously with ApIII and fluo-3 (calibrated in terms of Ca^{2+}-bound dye). Traces in Fig. 2 *B* correspond to the $[Ca^{2+}](t)$ derived from the signals, assuming for ApIII k_{OFF} = 700 s^{-1} (Baylor, Quinta-Ferreira, and Hui, 1985) and k_{ON} = 0.025 s^{-1} μM^{-2} (Kovacs et al., 1983), and for fluo-3 k_{OFF} = 90 s^{-1} and k_{ON} = 80 s^{-1} μM^{-1}. The same procedure was used with calcium green-1, yielding k_{OFF} = 30 s^{-1}, and k_{ON} = 120 s^{-1} μM^{-1}. In different experiments, fluo-3 rate constants fitted in this way varied within a factor of two of these values.

When ApIII and a fluorescent dye were present inside the cells, both the measurement of dye concentrations and the calculation of $[Ca^{2+}]$ and [dye-bound Ca^{2+}] had to be changed. The concentrations of the fluorescent dye (D_1) and ApIII (D_2) were derived from measurements of fiber absorbance in the center of the fiber, at 510 nm and 550 nm (a convenient peak of ApIII absorbance), performed at 10-min intervals during the experiment. The concentrations were derived from the following expressions for resting absorbancies:

$$A_{510} = A_{510}(0) + f\ p\ (D_1\ \epsilon_{1,510} + D_2\ \epsilon_{2,510})$$
$$A_{550} = A_{550}(0) + f\ p\ (D_1\ \epsilon_{1,550} + D_2\ \epsilon_{2,550}), \qquad (4)$$

where $A_\lambda(0)$ is the absorbance measured at the beginning of the experiment, when there is no dye in the fiber, and f is 0.7, the fraction of fiber volume available for dye diffusion (Baylor et al., 1983). A data conversion program interpolated linearly between two successive measurements of concentration to calculate the concentration at the time of each record.

The formulas for calculation of $[Ca^{2+}]$ and [dye-bound Ca^{2+}] were changed to account for the presence of two dyes as follows. $[Ca^{2+}]$ was still calculated through Eq. 1 or 3, but F_{min} was calculated with Eq. A4 and A6 (Appendix A). An approximate value is

$$F_{min} = F_b + 0.75\ q_{min} I_0 \frac{D_1\ \epsilon_{1,\lambda}}{C_1 + C_2} \{1 - \exp[-\ln 10\,(C_1 + C_2)\,p]\}\,d \qquad (5)$$

with $C_1 = D_1\ (\epsilon_{1,490} + \epsilon_{1,530})$, and $C_2 = D_2\ (\epsilon_{2,490} + \epsilon_{2,530})$. $\Delta[Ca^{2+}]$ was also calculated from the ApIII signal at 720 nm.

Depletion and Calcium Content of the SR

From the release flux waveform, a waveform corrected for depletion of calcium in the sarcoplasmic reticulum was calculated by the method of Schneider et al. (1987). The correction procedure assumes that the slow decay of calcium release flux that follows the initial fast relaxation is caused by depletion of Ca^{2+} in the SR. The depletion correction yields a waveform that reflects the kinetics of the SR permeability, rather than its contents, and gives an estimate of total [Ca] in the SR before the pulse ($[Ca]_{SR}$).

Solutions

Compositions of external and internal solutions used in most experiments are in Table I. The main difference in the internal solutions is the use of 15 mM EGTA in frogs and 8 mM in rats. This was dictated purely by experience, the concentrations being minimal for suppressing contractile movement. In many experiments, 2–3 mM of fluorescent indicator (either calcium green-1 or fluo-3, both from Molecular Probes, Inc., Eugene, OR) were included. Final osmolality was adjusted with glutamic acid, and final pH was adjusted with CsOH. For frogs, the osmolality of the internal so-

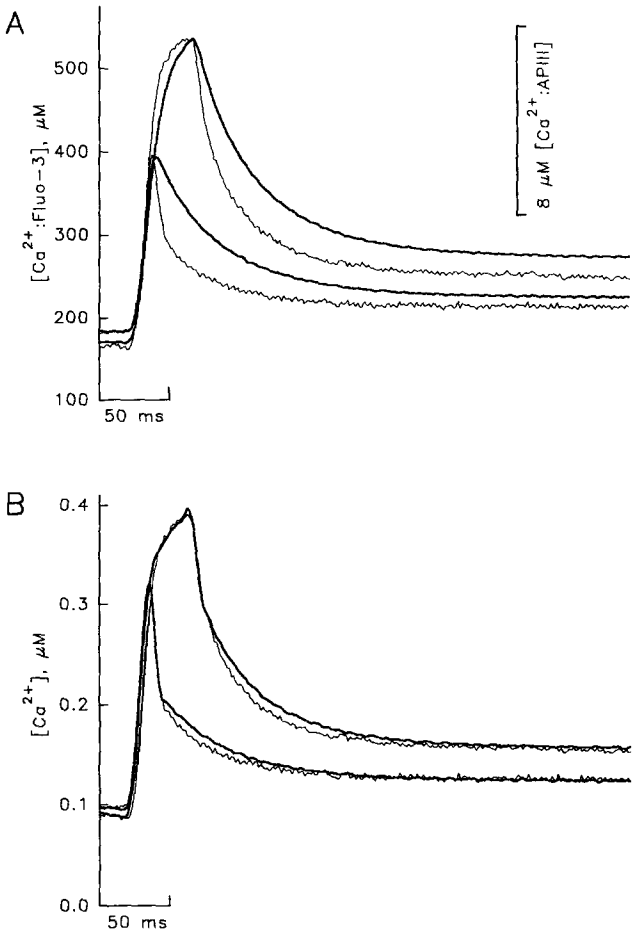

FIGURE 2. Determination of the kinetics of fluo-3. The kinetic rate constants of fluo-3 were determined by simultaneously measuring ApIII and fluo-3 signals. (*A*) Fluorescence intensity (*thick lines*) and the increase in ApIII absorbance (that is, absorbance increase at 720 nm corrected for the intrinsic absorbance change as described by Brum et al., 1988). The transients were elicited with pulses of 20 and 50 ms to −30 mV from hp (−90 mV). The signals were scaled to match their amplitudes and calibrated in terms of Ca^{2+}-bound dye. Because the ApIII (absorbance) signals only contain information regarding increment in Ca^{2+}-bound dye, they were shifted to the baseline provided by the fluorescence signals. (*B*) $[Ca^{2+}](t)$ derived from the fluorescence signals in *A* (*thick lines*) or $\Delta[Ca^{2+}](t)$ from the absorbance signals in *A*. The derivation used Eq. 3 and the kinetic constants of ApIII given in the text. The kinetic constants for fluo-3 were adjusted by trial and error to obtain the best agreement in the records shown and four other records. The best values, judged by eye, were k_{ON} = 80 $\mu M^{-1}s^{-1}$ and k_{OFF} = 90 s^{-1}. In this and all other figures the external solutions were the same (Table I). The internal solutions present in the end pools of the chamber contained 0.8 mM ApIII and 1.0 mM fluo-3 and a nominal $[Ca^{2+}]$ of 100 nM. When the records were obtained, the concentrations measured in the fiber were [fluo-3], 1.02 mM; [ApIII], 1.6 mM. Fiber 1337, frog; diameter, 94 μm; path, 58 μm; sarcomere length, 3.8 μm; linear capacitance, 11.5 nF.

lutions was 260 mosmol/kg and that of the external solution was 270 mosmol/kg. For rats, all solutions had 300 mosmol/kg. The solutions for frog muscle were set at room temperature to pH 7.0, and those for rat fibers were adjusted to pH 7.2. Except for the ones in which temperature was the variable, all experiments with frog fibers were carried out at 12°–14°C; those with rat fibers were at 14°–16°C.

RESULTS

Ca^{2+} Release Flux in Studies with the Absorption Dye

Calcium transients measured with ApIII in frog and rat fibers are illustrated in Fig. 3 *A*. Transients were elicited by a pulse to −40 mV from −90 mV (holding potential, hp) for the frog fiber represented, and to the same voltage from −80 mV hp for the rat fiber. In the presence of a high concentration of the slowly equilibrating Ca^{2+} buffer EGTA, the shape of Ca^{2+} transients is similar to the Ca^{2+} release waveform (Ríos and Pizarro, 1991). As shown, Ca^{2+} transients measured in rat fibers were usually smaller and less peaky than in frog fibers at this voltage The internal solution composition was not exactly the same (15 mM EGTA in frogs, 8 mM in rats), but we believe this was not the cause of the difference in release.[1]

Because release flux is crucial for the present work and it had different characteristics in the two previous reports (Delbono and Stefani, 1993; García and Schneider, 1993), we illustrate here in detail the steps used to derive it by two different methods. In many experiments, the release flux was estimated by the method of Melzer et al. (1987). A Ca^{2+} removal model was simultaneously fitted to the decay of Ca^{2+} transients elicited by pulses of different durations and amplitudes. Thick lines in Fig. 3 *A* represent the best-fit theoretical Ca^{2+} transients. The sets of removal parameters for best fit (see legend for Fig. 3) were very similar for frog and rat fibers. The calculated Ca^{2+} release fluxes are shown in Fig. 3 *B*. Since in both fibers there was little variation in release flux after the initial phase of inactivation, we interpreted that the release elicited by this low-voltage pulse did not cause appreciable depletion in either experiment. Release flux was almost threefold greater in the frog fiber experiment, and the ratio of peak over steady release was almost twofold greater.

Ca^{2+} transients were measured at different test voltages and are shown in Fig. 4 *A* for two other fibers. The Ca^{2+} transients measured in frog fibers were consistently larger and had a greater peak. The corresponding Ca^{2+} release flux waveforms were almost 10-fold greater in the frog fibers at all voltages (Fig. 4 *B*). The initial peak was present at all but the lowest voltages. At potentials above −30 mV, the release flux records had an additional slow decay, which was interpreted as caused by depletion of Ca^{2+} in the SR (Schneider et al., 1987). In those cases the correction procedure introduced by these authors was used, which led to records with a constant level of release after the peak. In these corrected records it was therefore possible to define a peak and a steady level (R_p and R_s). For the records of Fig. 4, these values are represented versus pulse voltage in Fig. 5 *A*. Ratios R_p/R_s are in Fig. 5 *B*. In rat fibers, the ratio was essentially independent of voltage. On the contrary, in frog fibers it was strongly voltage dependent, as shown. Regardless of voltage, R_p/R_s was greater in frog fibers.

TABLE I
Solutions

	Frogs		Rats	
Solution	Internal	External	Internal	External
ApIII	0.8	—	1.6	—
ATP	5.0	—	5.0	—
Ca	*	10.0	*	2.0
CH_3SO_3	—	130.0	—	154.0
Cs	125	—	160.0	—
EGTA	15.0	—	8.0	—
Glutamate	100.0	—	145.0	—
Mg	5.5	—	5.5	2.0
TEA	—	122.5	—	150.0

Concentrations are in millimolar.
*The internal solutions had calcium added for a nominal [Ca^{2+}] of 50–100 nM. Internal solutions had 5 mM glucose and 5 mM phosphocreatine. External solution had 1 μM TTX, 1 mM 3,4-diaminopyridine, and 1 mM 9-anthracene carboxylic acid. All solutions had 10 mM HEPES.

Ca^{2+} Transients and Release Flux Derived from Fluorescence Signals

Two of the experiments with fluorescent dyes are illustrated in Fig. 6, which shows in panels *A* Ca^{2+} transients derived from fluorescence signals of calcium green-1 (frog) and fluo-3 (rat). The two methods of calculation of Ca^{2+} release flux are illustrated in panels *B*. Solid lines represent release flux calculated from Ca^{2+} transients of Fig. 6 *A* with the removal method. The model of removal of Ca^{2+} in this case had an additional term, Ca^{2+} binding to the fluorescent dye. As shown, the peak of release in frog experiments was up to 15-fold greater than the steady level. In the rat experiment shown, the ratio ranged between 1.8 and 2.4 at voltages from −40 to −10 mV.

As discussed in Methods, in situations where the fluo-

[1]Provided that the [dye] in the internal solution was small, no systematic differences were observed with the passage of time during an experiment, when [EGTA] inside the cells went from nearly 0 to equilibrium with the end pools. This is consistent with the expectation that a slowly reacting buffer should not affect concentrations very close to open channels (Stern, 1992).

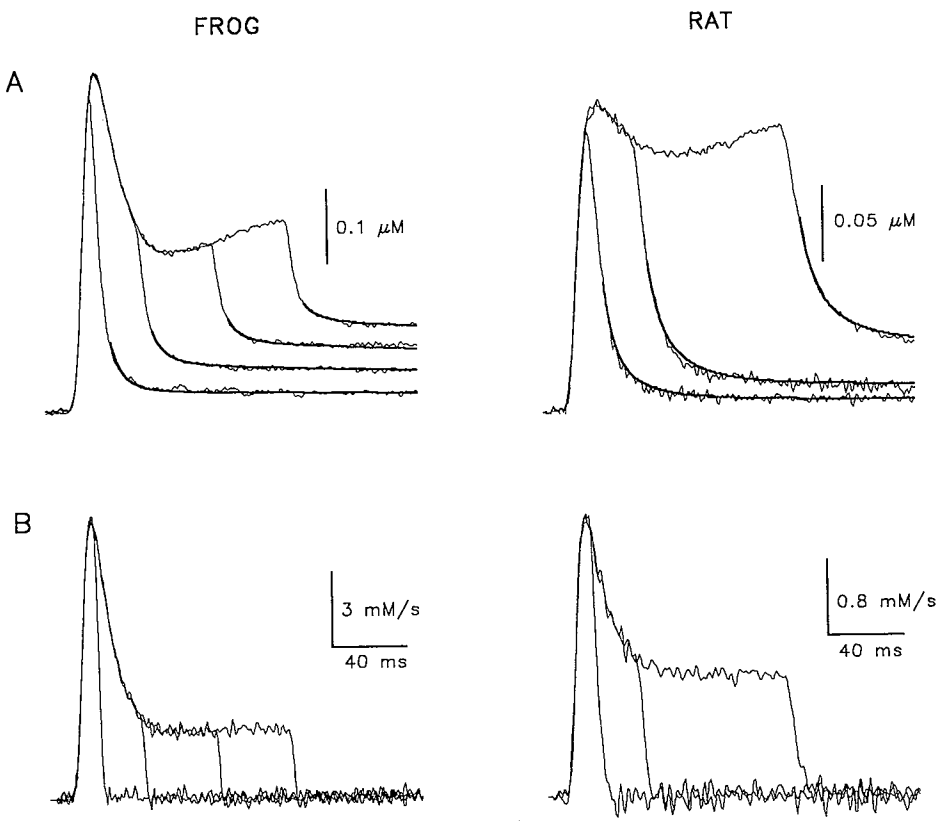

FIGURE 3. Ca^{2+} transients and flux, determined with an absorption dye. (*A*) Records in the thin trace represent $\Delta[Ca^{2+}](t)$ determined with ApIII. Transients were elicited with pulses to −40 mV from hp (−90 mV in frog, −80 mV in rat). Note that Ca^{2+} remains elevated after the pulse and takes seconds to return to the baseline level, as consistently observed in the presence of EGTA. The durations used were, in frog, 20, 50, 100, and 150 ms; in rat, 20, 50, and 150 ms. Transients in response to other voltages and durations were also included in the fit. Thick lines represent the theoretical $\Delta[Ca^{2+}](t)$ predicted by the removal model during determination of release flux. Of the removal model parameters, six were selected by a nonlinear least squares routine to fit the records shown and several others. (*B*) Release flux, calculated as the sum of the time derivative of $[Ca^{2+}](t)$ and the removal flux. The removal flux was calculated as the response of the removal model, fitted as shown in *A*. The fitted parameters and their values for the frog fiber were [EGTA], 12 mM; $k_{ON\ Ca\ EGTA}$, 1.1 $\mu M^{-1}s^{-1}$; $k_{OFF\ Ca\ EGTA}$, 4.1 s^{-1}; maximum pump rate, 1 mMs^{-1}. For the rat fiber: [EGTA], 2 mM; $k_{ON\ Ca\ EGTA}$, 1.1 $\mu M^{-1}s^{-1}$; $k_{OFF\ Ca\ EGTA}$, 3.4 s^{-1}; maximum pump rate, 1 mMs^{-1}. The other parameters had standard values in all experiments. For frog fibers: $k_{ON\ Ca\ Trop}$, 125 $\mu M^{-1}s^{-1}$; $k_{OFF\ Ca\ Trop}$, 1,200 s^{-1}; $k_{ON\ Ca\ Parv}$, 100 $\mu M^{-1}s^{-1}$; $k_{ON\ Mg\ Parv}$, 0.03 $\mu M^{-1}s^{-1}$; $k_{OFF\ Ca\ Parv}$, 1 s^{-1}; $k_{OFF\ Mg\ Parv}$, 3 s^{-1}; $K_{D\ pump}$, 1 μM; [pump Ca^{2+}-binding sites], 100 μM; [troponin], 240 μM; [parvalbumin], 1 mM. For rat fibers: $k_{ON\ Ca\ Trop}$, 130 $\mu M^{-1}s^{-1}$; $k_{OFF\ Ca\ Trop}$, 1,000 s^{-1}; $k_{ON\ Ca\ Parv}$, 160 $\mu M^{-1}s^{-1}$; $k_{ON\ Mg\ Parv}$, 0.04 $\mu M^{-1}s^{-1}$; $k_{OFF\ Ca\ Parv}$, 0.5 s^{-1}; $k_{OFF\ Mg\ Parv}$, 3 s^{-1}; $K_{D\ pump}$, 2 μM; [pump Ca^{2+}-binding sites], 150 μM; [troponin], 250 μM; [parvalbumin], 0.7 mM. Frog fiber 1143: diameter, 105 μm; linear capacitance, 16.5 nF; sarcomere length, 2.5 μm. Rat fiber 1239: diameter, 41 μm; linear capacitance, 5 nF; sarcomere length, 4.4 μm.

rescent dyes are at concentrations >∼500 μM, a minimum of release flux can be estimated as the time derivative of Ca^{2+} bound to the dye. When the records in Fig. 6 were obtained, the concentration of fluo-3 was 1.6 mM and the concentration of calcium green-1 was 600 μM, and the conditions for predominance of removal by the fluorescent dye were satisfied. The records plotted with dashed lines in Fig. 6 *B* are the time derivatives of Ca^{2+} bound to the fluorescent dye. The estimate is less than but close to the one obtained by the removal method. In this way and in many experiments, it was confirmed that the ratio of peak to steady release was greater in frog muscle.

24 experiments with frog muscle fibers and 17 with rats are summarized in Table II. The main entries in the table are the peak and steady values of release flux, R_p and R_s, at the highest voltage applied, and their ratio. In frogs, stretching to beyond 3.5 μm/sarcomere caused a modest decrease of release flux and ratios at all voltages. In rats, no effects were detected up to sarcomere lengths of 4.4 μm. It was extremely difficult to prevent movement in rat fibers at slack length, so that the values of release flux listed were obtained at low voltages (up to −30 mV) and are not to be compared with the maximum values obtained with stretched fibers.

In some experiments of each group, fluorescent dyes were present and used to simplify the estimation of release flux as described. There was no appreciable difference in the results obtained with both methods.

For both species, the linear capacitance C_m was determined (as a measure of membrane area) with positive pulses from 0 mV hp and with pulses to −110 mV from −90 mV hp. The values did not differ by >15%, and the lowest value (at 0 mV hp) is listed. In the conditions of homogeneous membrane polarization used here, this linear capacitance is proportional to the area of surface plus transverse tubule membrane.

From C_m and the measured geometry of the fibers,

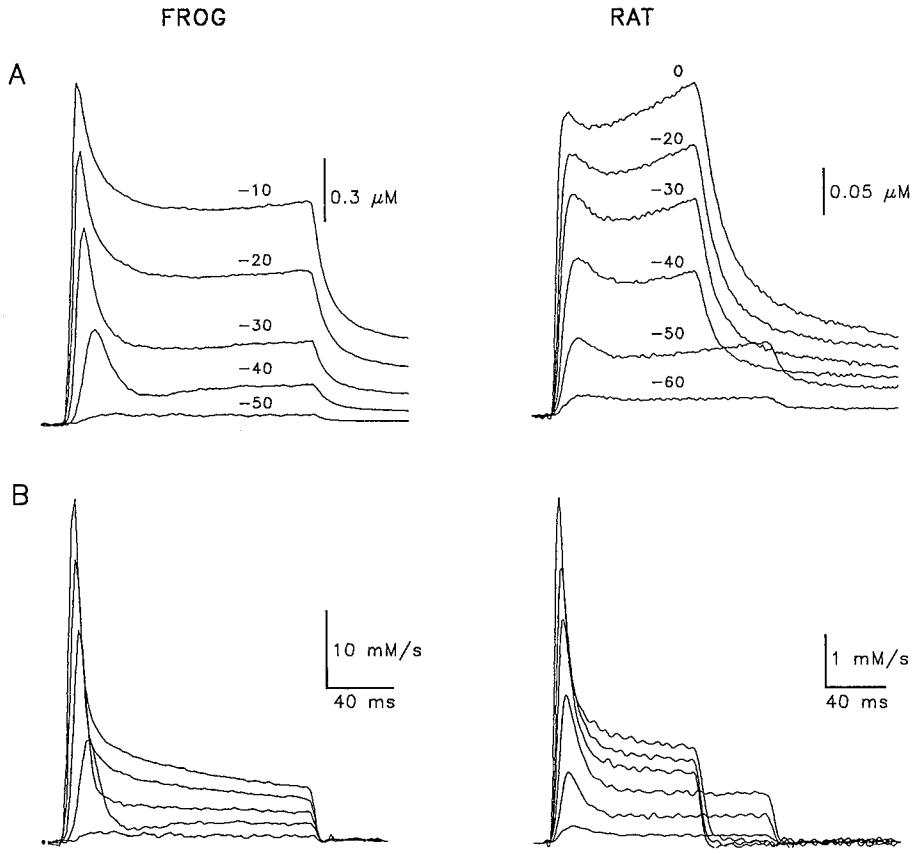

FIGURE 4. $[Ca^{2+}]$ transients and release compared at different voltages. (*A*) $\Delta[Ca^{2+}]$ elicited from hp to the voltages indicated. (*B*) Ca^{2+} release flux derived from the records in *A*. Parameters of the removal model for the frog fiber: [EGTA], 10 mM; $k_{ON\ Ca\ EGTA}$, 0.5 $\mu M^{-1}s^{-1}$; $k_{OFF\ Ca\ EGTA}$, 5.0 s^{-1}; maximum pump rate, 1 mM s^{-1}. For the rat fiber: [EGTA], 6 mM; $k_{ON\ Ca\ EGTA}$, 0.9 $\mu M^{-1}s^{-1}$; $k_{OFF\ Ca\ EGTA}$, 4.5 s^{-1}; maximum pump rate, 1 mM s^{-1}. Frog fiber 1111: diameter, 102 μm; linear capacitance, 13 nF; sarcomere length, 2.5 μm. Rat fiber 1244: diameter, 33 μm; linear capacitance, 4 nF; sarcomere length, 4.3 μm.

taking into account that the surface area is incremented ~80% over the geometric area of the cylinder by caveolae and foldings (Dulhunty and Franzini-Armstrong, 1975), we estimated transverse tubule membrane density per unit fiber volume (A_T/V_f) to be 0.48 μm^{-1} for frog fibers and 0.61 μm^{-1} for rat fibers. These values are greater than the values determined by morphometry, both for frog sartorius (0.22 μm^{-1}; Franzini-Armstrong, 1972) and mouse EDL (0.41 μm^{-1}; Luff and Atwood, 1971), but both techniques give higher T tubule membrane density for the mammal, as expected from the existence of two sets of T tubuli per sarcomere in mammalian muscle and only one in frogs.

Table II shows that on average, the peak release flux for large pulses is about fivefold greater for frog fibers, whereas the steady release flux is about threefold greater. The differences are significant at the 0.001 level in two-tailed *t* tests. The estimated flux ratio of peak to steady release was between twofold and fourfold greater in frog fibers, depending on the test volt-

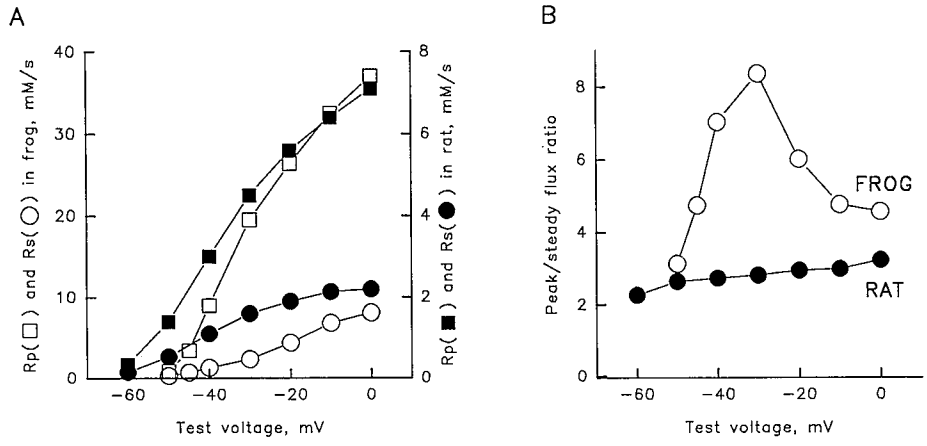

FIGURE 5. Voltage dependence of flux components and their ratios. (*A*) Peak (*squares*) and steady values of release flux (*circles*), for frog (*open symbols*) and rat, derived from the records of Fig. 4 *B* after correction for depletion. Steady values are averages of release flux during the last 20 ms of the pulses. (*B*) Ratios of peak and steady values in *A*.

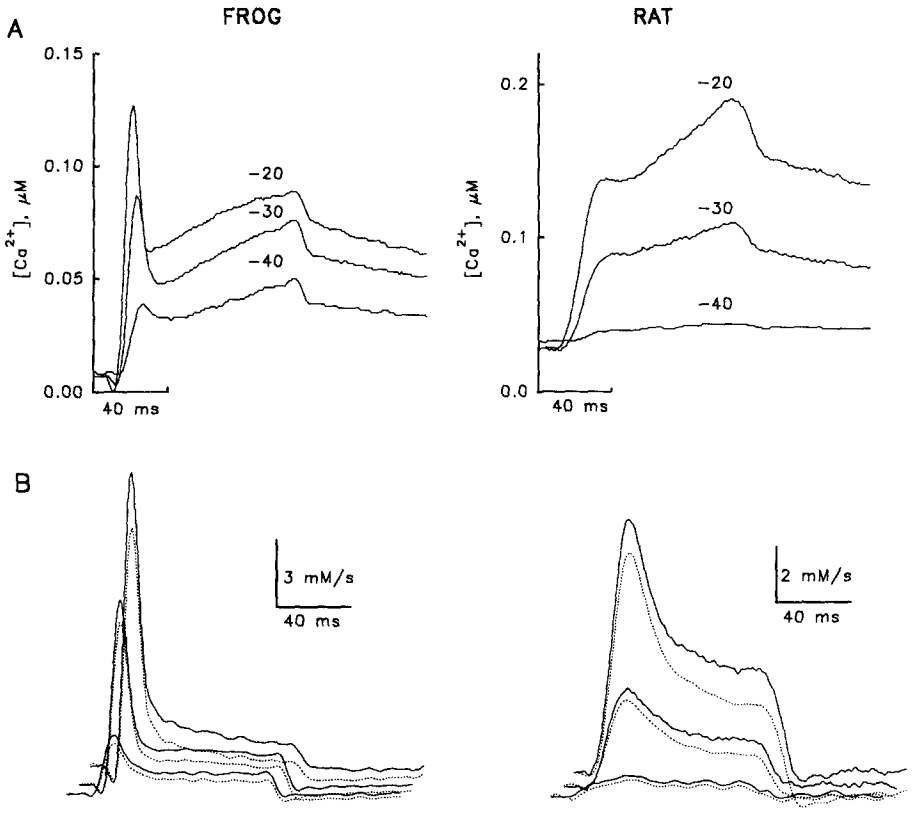

FIGURE 6. Ca^{2+} transients and flux determined with fluorescence indicators. (*A*) $[Ca^{2+}](t)$ determined from fluorescence of calcium green-1 in a frog fiber and with fluo-3 in a rat fiber. 100-ms test pulses were applied from hp to the voltages indicated. While the records were taken, [calcium green-1] went from 540 to 670 μM, whereas in the rat fiber [fluo-3] went from 1,530 to 1,670 μM. (*B*) Ca^{2+} release flux by two methods. Continuous lines represent in both panels the release flux calculated with the removal method. Dashed lines plot the time derivatives of Ca^{2+} bound to the fluorescent dye, derived from the signal using text Eq. 1. Given the high dye concentration and their speed of reaction, most of the released Ca is taken up by the dyes, and their binding rate provides a close minimum estimate of release flux. In particular, peak release and peak derivative of dye-bound Ca^{2+} differ by <30% when [calcium green-1] is 500 μM or greater. There was no EGTA in the internal solutions, and $[Ca^{2+}]$ was added for a nominal 50 nM. Frog fiber 1192: diameter, 80 μm; linear capacitance, 20.0 nF; sarcomere length, 2.9 μm. Rat fiber 1227: diameter, 55 μm; linear capacitance, 6.5 nF; sarcomere length, 3.8 μm.

age. The differences are significant at the 0.05 level at all voltages.

When release flux is normalized to T tubule area, the difference becomes even greater. For the frog fibers, the normalized flux is 19 μm mM/s (or 1.9×10^{-17} mol/s and square micron of transverse tubule), whereas for the rat it is 4.9 μm mM/s.

Table II also lists an estimate of $[Ca]_{SR}$ for every group of experiments as given by the depletion correction procedure (Schneider et al., 1987). On average, $[Ca]_{SR}$ was 3.4 mM (SEM = 0.6 mM) in frogs and 1.9 (0.3) mM in rats. This difference was not significant ($P = 0.06$) in a one-tailed t test.

Knowing $[Ca^{2+}]$ in the SR, we estimated SR permeability during the steady release phase. The ratio Ca^{2+} release flux (R_s) over $[Ca]_{SR}$ is, under simple assumptions, equal to the permeability P of the SR membrane multiplied by the surface-to-volume ratio of the SR (Shirokova et al., 1995). We used our estimate of T tubule area per unit myoplasmic volume (A_T/V_f in the tables), together with the volume density of the SR, (V_{SR}/V_f) (estimated at 0.09 for frogs and rats; Eisenberg, 1983), to obtain a meaningful permeability:

$$(R_S/[Ca]_{SR})\,(V_{SR}/V_f)\,(A_T/V_f) = [P/(V_{SR}/A_{SR})]\,(V_{SR}/V_{SR}) = P \times (A_{SR}/A_T).$$

The value $P \times (A_{SR}/A_T)$ is listed as the last column in Table II. It is the SR membrane permeability during the steady phase of release, multiplied by the ratio of SR to T membrane areas. If we assume that release is restricted to the junctional area of the SR, and consider that this area is about the same as the T membrane area, the value $P \times (A_{SR}/A_T)$ constitutes the permeability of the junctional SR membrane, which is essentially a measure of density and open probability of the release channels involved in the steady phase. This permeability is about threefold greater in frog fibers than in rat fibers. Summarizing the quantitative comparisons, the steady release flux is about threefold greater in frog fibers, flux density per unit area of T tubule is fourfold greater, and permeability during the steady phase is threefold greater. Peak release flux is about fivefold greater in the frog fibers.

Given the voltage dependence of the flux ratio in

TABLE II

Release Flux in Frog and Rat Fibers

	C_m,	Path	Diameter	$[Ca]_{SR}$	R_p	R_s	Ratio	$Ratio_{max}$	A_T/V_f	$Px(A_{SR}/A_T)$
	nF	*μm*	*μm*	*mM*	*mM/s*	*mM/s*			μm^{-1}	$cm\ s^{-1}\ 10^{-4}$
Frogs (slack)	20.3	99.8	115.5	4.0	35.4	9.6	3.6	6.6	0.41	0.93
SEM (n = 13)	(0.9)	(4.9)	(7.6)	(0.9)	(5.1)	(1.5)	(0.2)	(0.8)	(0.04)	(0.15)
Frogs (stretch.)	12.4	72.0	68.3	2.6	24.9	8.5	3.1	4.6	0.57	0.56
SEM (n = 11)	(1.5)	(1.5)	(6.4)	(0.6)	(4.8)	(1.8)	(0.3)	(0.3)	(0.07)	(0.06)
Frogs average	16.7	87.0	93.8	3.4	30.6	9.1	3.4	5.8	0.48	0.76
SEM (n = 24)	(1.2)	(4.5)	(7.0)	(0.6)	(3.6)	(1.1)	(0.2)	(0.5)	(0.04)	(1.0)
Rats (slack)	6.9	46.6	48.6	—	0.7	0.4	1.8	—	0.6	—
SEM (n = 5)	(0.4)	(3.7)	(5.8)		(0.3)	(0.1)	(0.1)		(0.08)	
Rats (stretch.)	6.9	45.6	46.8	1.9	7.0	3.0	2.3	—	0.61	0.29
SEM (n = 12)	(0.5)	(2.3)	(2.7)	(0.3)	(1.7)	(0.7)	(0.2)		(0.04)	(0.06)

C_m is effective capacitance measured in depolarized fibers with pulses from 0 to 40 mV, or with pulses from −110 to −90 mV in fibers polarized at −90 mV. Path, represented by p in the text, is measured with micrometric vertical displacement of the microscope nosepiece, focusing at the top and bottom of the fiber. Diameter, d in the text, is measured with a micrometric eyepiece. $[Ca]_{SR}$ is derived from the depletion correction procedure and expressed in terms of myoplasmic H_2O. R_p and R_s are peak and steady values of release flux after correction for depletion, in a pulse to 0 or 10 mV (in frog fibers) and −10 mV (in rats). In slack rat fibers, R_p and R_s were measured at low voltages (up to −30 mV), because it was difficult to prevent movement. Ratio is R_p/R_s. $Ratio_{max}$ is the maximum measured ratio of peak to steady flux, always obtained at a test voltage of −40 or −35 mV. No $ratio_{max}$ is included for rats because the ratio was essentially the same at all voltages. A_T/V_f is the "area density" of transverse tubule membrane, derived from the measurement of capacitance as described in the text. $Px(A_{SR}/A_T)$ is the "effective" permeability of the junctional SR, defined in the text.

frog muscle, which is already clear in Fig. 5, Table II has an additional entry for frogs, the maximum ratio, obtained at or near −40 mV. This value was 1.5 to two-fold greater than the limiting value at high voltages.

Flux Ratios and Their Voltage Dependence

Table II shows that the ratio of peak to steady flux was consistently greater in frog fibers. The main difference, however, was in voltage dependence. Fig. 7 summarizes data on voltage dependence for 15 rat fibers and 18 frog fibers that were studied over a wide voltage range. The flux ratios were normalized to the maximal value for each fiber separately, then multiplied by the averaged maximum value. In rat fibers, the ratio was essentially voltage independent and averaged 2.2. In frog fibers, it had a maximum of ~5 at −35 mV, then decayed. Simple averaging obscured the voltage dependence because the maxima are located at somewhat variable voltages. In Fig. 7 *B*, the ratios were averaged after shifting so that the voltage for maximum ratios coincided.

Our working hypothesis is that a component of release is Ca^{2+} activated. The magnitude of this component should depend on the single-channel flux, as Ca^{2+} activation should depend on locally elevated $[Ca^{2+}]$ near open channels. This single-channel flux in turn depends on single-channel conductance and on the driving force (essentially, free $[Ca^{2+}]$ in the SR). Since $[Ca^{2+}]$ in the SR is buffered by fast, low-affinity buffers, free $[Ca^{2+}]_{SR}$ is probably proportional to total $[Ca]_{SR}$.[2] Determinations of $[Ca]_{SR}$ with electron probe microanalysis yield for the frog 1.5 mmol/kg cell water (Somlyo, Shuman, and Somlyo, 1977), but no equivalent studies exist for rats.

Our own estimates of $[Ca]_{SR}$ (Table II), which are close to the electron probe value, allowed us to look for correspondences between flux ratio and $[Ca]_{SR}$. This is done in Fig. 8; for frog fibers, open squares represent maximum ratios, and open circles, ratios at 0 mV. The lower ratios observed in rats (*solid symbols*) correspond to some extent to a lower $[Ca]_{SR}$. Thus, the lower flux per channel in rats might be explained in part by lower $[Ca]_{SR}$, and in turn explain the lower flux ratio. However, when data of individual species were considered, there was no correlation between SR content and flux ratio.

Effect of Temperature

The experiments described before were carried out within a narrow range of temperatures, 12°–14°C for frog fibers and 14°–16°C for rat fibers. However, rat muscles function at a much higher temperature. It is conceivable that rat fibers, if studied at 36°C, could have very different release flux waveforms.

Fig. 9 illustrates experiments designed to test this possibility, in which the temperature was changed very rapidly, using fast superfusion with solutions of different temperatures. The top panels present Ca^{2+} transients measured with ApIII. The records with thick

[2] In fact, the success of the depletion correction method of Schneider et al. (1988) indicates that the flux of release is close to proportional to $[Ca]_{SR}$, implying in turn that the single-channel current is close to proportional to $[Ca]_{SR}$ in the physiologic situation.

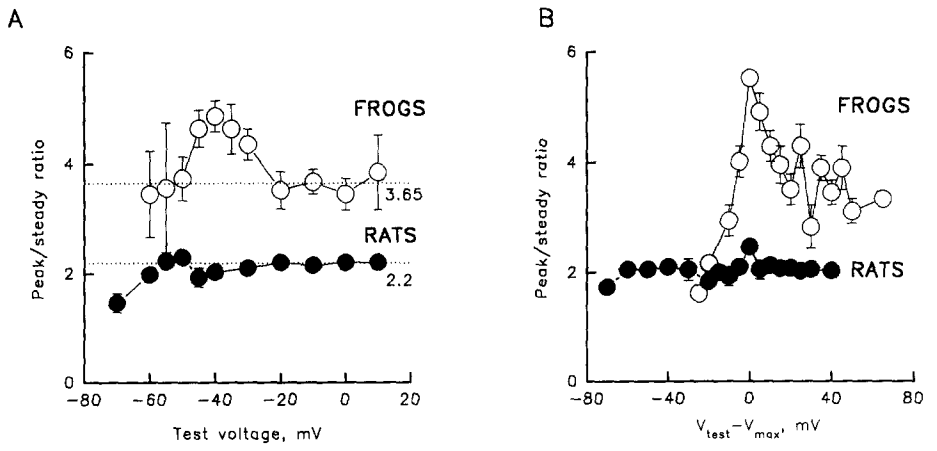

FIGURE 7. Averages of flux ratios. (*A*) Averages in 18 frog fibers (*open circles*) and 15 rat fibers (*solid circles*). Ratios were normalized separately to the maximum value in the experiment. The normalized ratios were then averaged, and the averages scaled by the average maximum ratio. Bars cover ± SEM. (*B*) The ratios were averaged after shifting, so that the voltage for maximum ratios coincided.

lines were obtained at low temperatures, 3°C for the frog fibers and 5°C for the rat fibers (measured with a thermistor placed very close to the fibers). The records with thin lines were obtained ~2 min later at 21°C.

Release flux records calculated with the removal method are represented in Fig. 9 *B*. As described in detail by González and Ríos (1993), when a high concentration of EGTA is present, the rate constants of the Ca^{2+}:EGTA reaction are the parameters of the removal model that most influence the fit. All transients obtained in the same species at a given temperature were well fitted with essentially the same parameters. However, different EGTA rate constant values were required at the different temperatures, and the values were somewhat different for the two species (details in legend to Fig. 9).

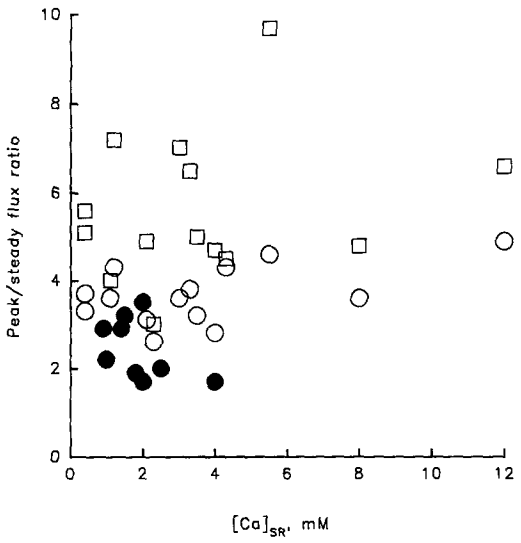

FIGURE 8. Release flux ratio and SR calcium content. Release flux ratio in frog experiments (*open symbols*), including maximum ratio (*squares*) and ratio at high voltage (*circles*), and ratio at high voltage in rat fibers (*solid circles*), plotted vs $[Ca]_{SR}$, obtained by depletion correction. For frogs, the correlation coefficients were 0.51 for the ratio at high voltage and 0.21 for the maximum, whereas for rats it was 0.49. The correlation was not significant in any case.

The effects of temperature on the two components of release flux and their ratio in rat fibers are represented in Fig. 10 *A*. The Q_{10} of peak release flux (*solid circles*) was > 3, that of steady release (*open circles*) was ~2.2, and that of their ratio (*squares*) ~1.6 in the experiment shown. All were rather insensitive to voltage. Fig. 10 *B* plots the average Q_{10} of ratios in six rat fibers. The average of all values at all voltages was 1.3.

We could not carry out these measurements in frog fibers over the same voltage range. At high temperatures and voltages above −30 mV, the ratios were sometimes smaller than at low temperatures. This was associated with (and probably caused by) the high release flux caused in the frog by voltages above −30 mV at high temperatures. The high release flux resulted in major depletion of Ca^{2+} in the SR, which made it difficult to determine the steady value of release flux. The Q_{10} of the ratio could be determined without these problems in one fiber, and the values went from 1.1 (at −30 mV) to 1.44 (at 10 mV).

In summary, in rat fibers, when the temperature went from 5 to 21°C, the ratio of peak to steady release went on average from 2.0 (SEM = 0.3, n = 4) to 2.5 (SEM = 0.5, n = 4). In frog experiments (at voltages of −30 mV or less) the ratio went from 3.6 (SEM = 0.1, n = 2) at 3°C to 4.7 (SEM = 0.2, n = 2) at 21°C. The temperature dependence of the release flux ratio thus appears to be moderate and similar in both species. This low temperature dependence makes it unlikely that the release flux ratio will be substantially different in rat muscle at 36°C. The flux ratio is fundamentally different in these two species, and the difference is not an artifact of studying the rat muscle at a nonphysiologic temperature.

DISCUSSION

The present results should be compared with two recent studies of release flux in rat fibers (Delbono

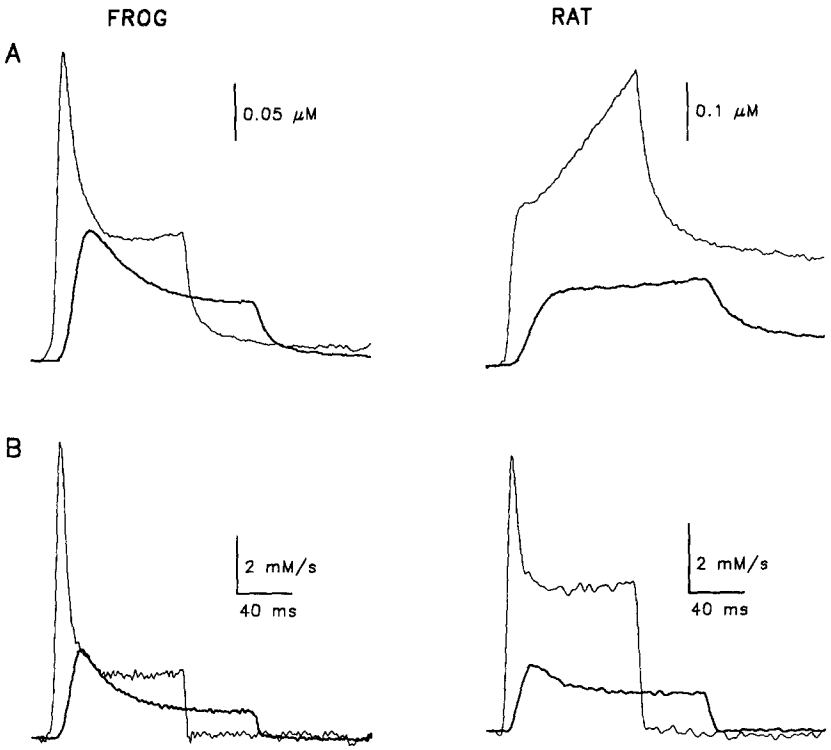

FIGURE 9. Effects of temperature. (*A*) $\Delta[Ca^{2+}](t)$ determined with ApIII at two temperatures in response to a pulse to −35 mV (frog) or −10 mV (rat). Records in thick trace were at low temperature, 3°C (frog) or 5°C (rat). Records in thin lines were obtained at 21°C. (*B*) Ca^{2+} release flux, determined by the removal method from the records at top. In these and all experiments at different temperatures, six parameters of the removal model were fitted and the others were set. The best fit values were, for the frog fiber at 3°C, $k_{ON\ Ca\ EGTA}$ = 0.9 $\mu M^{-1}s^{-1}$ and k_{OFF} = 3.1 s^{-1}; at 21°C, k_{ON} = 1.9 $\mu M^{-1}s^{-1}$ and k_{OFF} = 0.5 s^{-1}. [EGTA] was 7.5 mM and maximum pump rate, 1 mMs^{-1}. For the rat fibers at 5°C, $k_{ON\ Ca\ EGTA}$ = 0.8 $\mu M^{-1}s^{-1}$; k_{OFF} = 5.7 s^{-1}; at 21°C, k_{ON} = 1.7 $\mu M^{-1}s^{-1}$ and k_{OFF} = 10.9 s^{-1}. [EGTA] = 6 mM; maximum pump rate, 1 mMs^{-1}. Frog fiber 1275: diameter, 137 μm; linear capacitance, 16.0 nF; sarcomere length, 2.8 μm. Rat fiber 1290: diameter, 38 μm; linear capacitance, 4 nF; sarcomere length, 4.0 μm.

and Stefani, 1993; García and Schneider, 1993). Estimated release flux waveforms had different characteristics in the two. Those calculated by García and Schneider (1993) had peaks decaying monotonically to steady levels, similar to the ones obtained in frog muscle fibers by many investigators. In contrast, Delbono and Stefani (1993) deduced more complex waveforms, with characteristic second-rising phases after a peak that inactivated almost completely. The waveforms observed in rat fibers in the present work are devoid of second-rising phases. The magnitudes of peak and steady components are similar to those of García and Schneider (1993) and somewhat less than the ones obtained by Delbono and Stefani (1993).

Lower Release Flux in Mammalian SR

Peak release flux was about fivefold greater in frog than in rat muscle when determined with similar procedures at similar temperatures. The result was the same whether release flux was determined by either of two methods that involve different hypotheses. Steady release flux was also greater in the frog fibers, by threefold to fourfold. Again, this result was independent of the method used to estimate release.

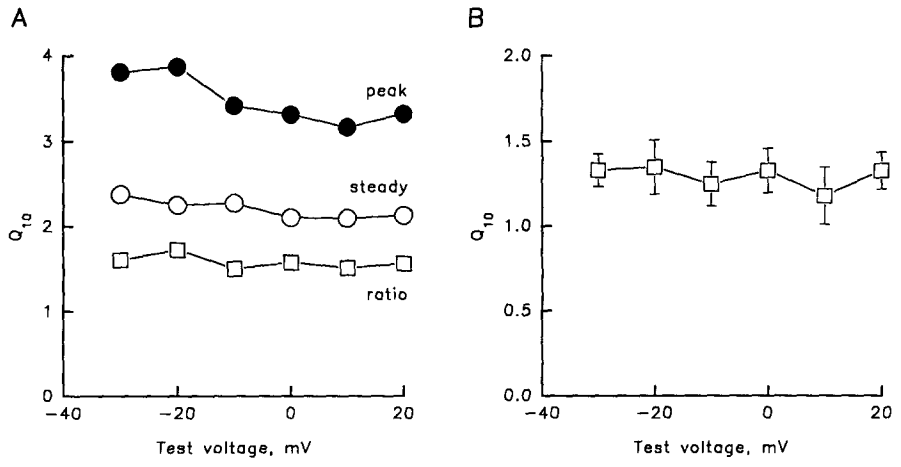

FIGURE 10. Voltage dependence of Q_{10}. (*A*) Q_{10} derived from measurements X at two temperatures as $[X(T_2)/X(T_1)]^{\alpha}$, with $\alpha = 10\ T_2/[(T_2 - T_1)(T_1 + 10)]$ for peak release flux (*solid circles*), steady release (*open circles*), and their ratio (*squares*) in a rat fiber. (*B*) Average Q_{10} of ratios determined in six identically prepared rat fiber experiments. In *A*, experiment 1291; diameter, 36 μm; linear capacitance, 4 nF; sarcomere length, 4.3 μm.

Since the single channel conductance in bilayers is similar for mammalian and amphibian species (Bull and Marengo, 1993; Smith et al., 1988), the lower value of the steady component of flux in rat muscle could be a result of lower values of any of the following: density of voltage sensors, density of SR channels, p_o, or driving force. In the following, we explore these possibilities.

In Table II are data on transverse tubule membrane area, derived from capacitance measurements. The area densities, 0.48 μm^{-1} (frog) and 0.61 μm^{-1} (rat), are consistent with the presence of two sets of transverse tubuli per sarcomere in the mammal. DHP binding densities given by Margreth et al. (1993) are in a similar ratio: 46 pmol/g of muscle for frog sartorius and 77 pmol/g for rat tibialis anterior. Therefore, the number of DHP receptors per unit membrane *area* appears to be the same, with the consequence that the number of voltage sensors per unit *volume* should be 1.5- to 2-fold greater in the rat fibers.

When release flux is expressed per unit of transverse tubule area, the difference between the two species becomes greater. In the frog fibers, steady release thus normalized is on average 20 mM/(s μm^{-1}), or 1.3×10^7 ions/s and square micron of transverse tubule, while for the rat it is 2.9×10^6.

An even greater difference is found if the release flux values are normalized to the density of DHP receptors. In the frog, steady release is 9.1 mM/s or 9.1 mmol Ca^{2+} per second and liter of myoplasmic H_2O. 46 pmol DHP sites per gram of muscle (Margreth et al., 1993) can be expressed in terms of myoplasmic water dividing by 0.58 (Baylor et al., 1983), as 79 pmol/g myoplasmic H_2O. The steady flux is therefore 0.11×10^6 mol of Ca^{2+} per mol of DHP receptor per second. In the rat fibers, assuming the same conversion factor, steady release would be 0.23×10^5 mol per mol of DHP receptor per second. If steady release was the function of release channels paired one to one with tetrads of voltage sensors, the average flux per channel would be $\sim 5 \times 10^5$ ions/s in the frog fibers and 10^5 ions/s in the rat fibers, well within the flux that single release channels carry in bilayer studies.

We also explored whether the difference in flux could be caused by a difference in driving force. Table II lists estimates of total [Ca] in the SR. These values were on average about twofold greater in the frog fibers, although there was a large dispersion in the results and the difference was not significant. Taking $[Ca]_{SR}$ into account, we obtained an estimate of permeability of the junctional SR, which was twofold to threefold greater in frog than in rat muscle.

In summary, the steady flux density (per unit membrane area or per DHP receptor molecule) as well as the permeability are all greater in the frog muscle. There is more steady flux per voltage sensor tetrad, either because the channels have greater p_o or because a greater number of channels in the SR contribute to the steady flux under the command of one tetrad.

An interesting teleologic consideration was suggested to us by Dr. Elizabeth Stephenson (UMD–New Jersey Medical School, Newark). In mammals, the transverse tubuli (and triadic junctions), at two per sarcomere, are next to the functional target of the released Ca^{2+}, troponin C in the areas of filament overlap. In frogs, there is one transverse tubule at the Z line, at a distance from the thick filament ends that can easily reach 0.5 μm. Therefore, much smaller gradients are necessary in the rat to drive Ca^{2+} diffusion for an equivalent activation of the contractile proteins. In this light, the fivefold difference in steady (and 10-fold difference in peak) flux per unit membrane area, which was at first a surprising result, may be a requisite for similar activation under very different geometries for Ca^{2+} diffusion. In this view, the double T tubule array of the mammal would not only be faster but metabolically more efficient, requiring lower gradients and lower Ca^{2+} flux overall.

Different Release Flux Ratios in Frogs and Rats

The two kinetic phases of Ca^{2+} release flux also have different *relative* magnitudes in frog and rat muscle. Most remarkably, in the frog muscle the ratio is strongly voltage dependent, whereas in the rat it is lower at all voltages and essentially constant, only falling below 2 at very low voltages. Although in both species the magnitudes of the components of flux depend strongly on temperature, the ratios do not, and the interspecies differences described above are found at all temperatures tested (3–22°C). This observation bears on the issue of sites for the two components of Ca^{2+} release, as the different flux ratios are roughly consistent with the different ratios of specific DHP to ryanodine binding.

When determined in isolated membrane fractions (Bers and Stiffel, 1993; Margreth et al., 1993; Anderson et al., 1994) and isolated tetrads (Anderson et al., 1990; Bers and Stiffel, 1993) of rabbit muscle, the DHP/ryanodine binding ratios ranged between 1.5 and 2.1. A single determination with human skeletal muscle gave a binding ratio of 2 (Margreth et al., 1993). Assuming one high affinity binding site per receptor (for both types), this corresponds to about four DHP receptors for every 2 feet of release channels, which is in agreement with predictions of the structural model of Block et al. (1988). In rat muscle homogenates, the only estimate is 1.2 (Margreth et al., 1993).

For frog muscle, the estimates of the ratio of DHP to ryanodine binding are consistently lower, ranging from 1.1 (Margreth et al., 1993) to 0.5 (Anderson et al.,

1994). Since only the mammalian ratio of specific binding is consistent with the general arrangement of proteins proposed by Block et al. (1989), one must imagine that the greater proportion of ryanodine receptors in amphibians corresponds to receptors that violate the pattern, either because they are outside the double row of junctional feet (consistent with observations of Dulhunty et al., 1992) or because the pattern of the stoichiometric arrangement observed in fish and mice does not apply to frog muscle, and the DHP receptors of frog muscle are fewer than in the scheme of Block et al. (1988).

A greater relative number of ryanodine receptors implies that more of them would be free from the direct influence of the voltage sensors. Since a mechanical contact is required in simple models of direct control but not for transmitter-mediated control, one would expect a greater importance of transmitter-mediated control in amphibian muscle. The present results are consistent with this expectation and the scheme proposed by Ríos and Pizarro (1988) in which release channels not directly controlled by voltage sensors contribute the peak component and are Ca^{2+} operated.

In this model, frog fibers would have comparatively greater peak release because they have more ryanodine receptor channels per voltage sensor. Specifically in the frog, at high voltages, when all voltage sensors are presumably activated, the difference between peak and steady levels of release flux relative to the magnitude of the steady component is 2.6 (3.6 − 1; Fig. 7). In rat muscle, and in the same units, the peak component of release is 1.2 (2.2 − 1; Fig. 10). These figures, 2.6 and 1.2, are in about the same proportion as the ryanodine/DHP binding ratios in frog and mammalian muscle. This result is consistent with the hypothesis of Ríos and Pizarro (1988), provided that the ratio between conductances of putatively Ca^{2+}-operated and voltage-operated channels is the same in both species.

Voltage Dependence of the Flux Ratio

A strong voltage dependence of the flux ratio is one of the most characteristic aspects of Ca^{2+} release in frog muscle. Below, we show that geometric aspects of the structural pattern of Block et al. (1988) plus simple hypotheses of local control by Ca^{2+} predict a voltage dependence in the flux ratio qualitatively similar to that observed.

Following Ríos and Pizarro (1988), we assume that the release channels paired with *V* sensors are strictly voltage operated and remain open for as long as the pulse is on. The unpaired release channels are Ca^{2+} operated. To account for the graded nature of release activation, we assume also that their opening does not result in opening of other Ca^{2+}-operated channels (this could be the result of a short open channel lifetime or of the greater distance between Ca^{2+}-operated channels than between them and their putatively voltage-operated neighbors). The operational consequence of this simplification is that the contribution to $[Ca^{2+}]$ of the Ca^{2+}-operated channels may be neglected. For simplicity we assume that the stimulus for channel opening is an increase in local $[Ca^{2+}]$ above a certain threshold. Consistent with the assumption of strict voltage dependence, the increase in local $[Ca^{2+}]$ contributed by a voltage-operated channel is assumed constant for the duration of the pulse, whereas the Ca^{2+}-operated channels contribute the "peak," that is, a brief opening or burst, added to the steady flux.

With these general hypotheses, the detail of the voltage dependence of the two components of release can be understood simply in terms of the geometry proposed by Block et al. (1988)[3] and illustrated in Fig. 11 *A*, displaying schematically voltage-operated channels (*V*) and Ca^{2+}-operated channels (*C*).

At all voltages, the ratio of release components will be equal to the ratio of C channels open over V channels open, multiplied by the ratio of their single-channel currents (an unknown quantity). At low voltages, when the V channels have very low p_o, the ratio will be determined by the *direct gain*—the number of Ca^{2+}-operated channels opened by one voltage-operated channel. As voltage increases, the p_o of the V channels increases, and the number of C channels that open increases more than proportionally, as $[Ca^{2+}]$ increases above threshold due to contributions from multiple V channels that overlap their areas of influence (*convergence*). As p_o increases further, the opportunities for convergent activation decrease, and a *redundance* effect comes into play, whereby increasing the number of V channels open cannot increase further the number of C channels open. In the limit of $p_o = 1$, the ratio of C channels open to V channels open should be proportional to the ratio of the total number of C channels to V channels (1 in the present assumptions). Intuitively, the ratio can be much greater at intermediate p_o.

Fig. 11 *B* illustrates an implementation of this model, carried out in the simplest quantitative terms, to show that the intuitive concepts of convergence and redundance can indeed explain the observations. The quantitative aspects are described in Appendix B.

As shown by the simulation in open symbols, the model gives a reasonable reproduction of the voltage dependence observed in frog fibers, with its stages of

[3] Qualitatively similar results are still obtained after relaxing some aspects of the pattern, to allow, for instance, for the presence of additional Ca^{2+}-operated release channels, as proposed by Dulhunty et al. (1992).

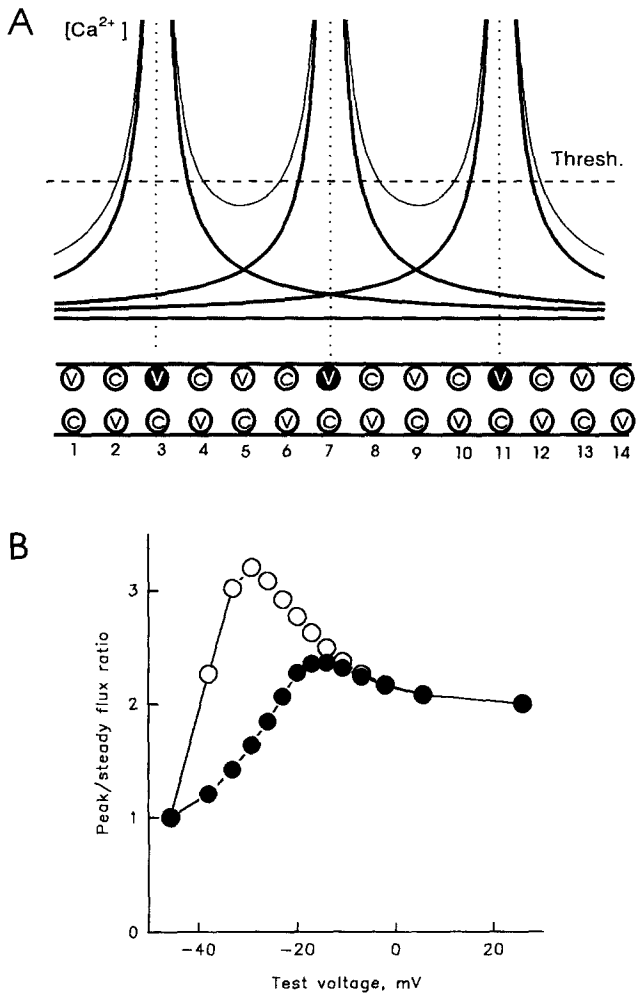

FIGURE 11. A model of dual control of release. (*A*) The diagram, inspired by the structural model of Block et al. (1988), consists of 14 V and 14 C channels forming a double row, with 30 nm interchannel distance. Channels V face jT tetrads in the transverse tubule and are supposed to be directly and exclusively controlled by voltage sensors. Channels C are not paired with jT tetrads and are supposed to be activated by Ca^{2+}. A detailed description of the calculations is in Appendix B. The situation represented in the diagram is with three V channels open. The curves at top represent the $[Ca^{2+}]$ contributed by the individual open channels (*thick trace*, calculated with Eq. B1) and the total $[Ca^{2+}]$, obtained by superposition (*thin trace*). The horizontal line represents a threshold level that is compared with $[Ca^{2+}]$ to determine whether each C channel will be open or closed. The diagram represents one of the many configurations with 3 V channels open ($n_V = 3$). For every configuration the number of C channels open was determined, then averaged over all configurations with 3 V channels open to yield an average number of C channels open $[n_C(n_V = 3)]$. This was repeated for all possible values of n_V, thus yielding the function $n_C(n_V)$, from which the predicted ratio could be derived. (*B*) Model-predicted flux ratio, $(n_C + n_V)/n_V$, mapped to the voltage axis. Values in open symbols obtained with parameters $Q_0 = 30$ μM nm, $Q_1 = 650$ μM nm, $\lambda = 34$ nm and threshold = 10 μM. The solid symbols were obtained reducing Q_1 and Q_0 to 0.7 of the original values.

convergence and redundance. It cannot, however, reproduce the ratio in mammalian muscle. The filled symbols were obtained by reducing the individual channel flux to represent the lower flux and permeability observed in the rat fibers. Some of the differences in voltage dependence were reproduced, especially the reduction in overall gain and peak of the voltage-dependent ratio, but the main feature introduced was a domain in which the ratio increases markedly with voltage. Other parameter changes also failed to generate the essentially voltage-independent ratio observed with rat fibers. This makes sense intuitively, as it seems impossible to have a set of equally prepared Ca^{2+}-operated channels in a linear lattice and have neither convergence nor redundance in activation.

These differences in the voltage dependence of the ratio suggest that there are fundamental differences between species. The finding that two functionally and structurally different isoforms of the ryanodine receptor are present at comparable densities in frog (Lai et al., 1992; Murayama and Ogawa, 1992; Conti et al., 1995), but not mammals (Lai, Erickson, Rousseau, Liu, and Meissner, 1988; Takeshima, Nishimura, Matsumoto, Ishida, Kangawa, Minamino, Matsuo, Udea, Hanaoka, Hirose, and Numa, 1989; Conti et al., 1995) underscores that the mechanisms of control could be qualitatively different, and different from the one contemplated in the present scheme.

The Effect of Temperature

The present results show that in both species, release increases markedly with temperature. Although this could be studied in rat muscles over a wide voltage range, it could only be studied at lower voltages in frogs, given the rapid depletion of Ca^{2+} in the SR that occurred when frog fibers were activated with high voltage pulses at high temperature. Within these limitations, however, there were no differences in the dependence of release with temperature between the species.

Peak release increased close to threefold for a 10°C increase in temperature. At the same time, steady release flux increased by a factor of ~2.3. Consequently, the flux ratio only increased, on average, by a factor of 1.3. These numbers were about the same at all voltages studied.

That the magnitude of both components increased in a similar proportion, so that their ratio increased only slightly, is consistent with the idea that the two components correspond to "hard-wired" mechanisms, like flux through physically distinct channels. A purely kinetic mechanism, in which the steady release corresponds to steady inactivation in an ensemble of channels, would have to be affected in a peculiar way by temperature in order to reproduce the present observation.

APPENDIX A

Detection of Ca^{2+} with Two Dyes at High Concentration

This Appendix develops equations relating the fluorescence signal of Ca^{2+}-sensitive dyes to $[Ca^{2+}](t)$ when two dyes are present at concentrations that absorb both the exciter and emitted light nonnegligibly. This extends a treatment of Klein et al. (1988) to a two-dye case. It also generalizes the treatment to an elliptical fiber geometry (instead of a rectangular section) and to "nonratioing" dyes. As in the above reference, this is a center ray analysis, assuming that propagation is always parallel to the optical axis, and neglecting all effects of finite aperture. In the present case this is probably a good approximation, since the epi-illumination and light collecting objective has a long working distance and intermediate numerical aperture (0.7).

The geometric aspects are illustrated in Fig. 12. Let $I(x,y,\lambda)$ represent excitation light intensity of wavelength λ, at position (x,y) inside the cell. This light has traversed a distance

$$u(x,y) = (b/a)\sqrt{(a^2 + b^2)} - y$$

within the fiber to reach from the point of entry at $(x, \sqrt{(a^2 - x^2)})$ to (x,y). $b = p/2$ and $a = d/2$ are half the vertical and horizontal transversal dimensions of the fiber. Accordingly, the light intensity will have attenuated from its incident value I_0 to

$$I(x,y,\lambda) = I_0 \exp[-\log 10\ (D_1 \epsilon_{1,\lambda} + D_2\ \epsilon_{2,\lambda})\, u] \tag{A1}$$

where D_1 and D_2 represent concentrations of the fluorescent dye and the absorption dye. The fluorescent intensity of wavelength λ_f, $dF(x,y,\lambda_f)$, excited in an element of volume $Ldxdy$ (where L is fiber length in the field) at (x,y), is

$$dF(x,y,\lambda_f) = q(\lambda,\lambda_f)\, I(x,y,\lambda)\, D_1 \epsilon_{1,\lambda} dx\ dy \tag{A2}$$

where $q(\lambda,\lambda_f)$ depends on the quantum efficiency of fluorescence at λ_f and incorporates other geometric aspects, such as fiber length in the field and numerical aperture. Of this intensity, the following portion will exit at the top of the fiber and be collected by the objective

$$dF_f(x,y,\lambda_f) =$$

$$q(\lambda,\lambda_f)\, I(x,y,\lambda)\, D_1 \epsilon_{1,\lambda}$$

$$\exp[-\log 10\,(D_1 \epsilon_{1,\lambda_f} + D_2 \epsilon_{2,\lambda_f})\, u]\, dxdy =$$

$$q(\lambda,\lambda_f)\ \ I_0 D_1 \epsilon_{1,\lambda} \exp[-\ln 10\,(C_1 + C_2)\, u]\, dxdy \tag{A3}$$

with $C_1 = D_1(\epsilon_{1,\lambda} + \epsilon_{1,\lambda f})$,

and $C_2 = D_2(\epsilon_{2,\lambda} + \epsilon_{2,\lambda f})$.

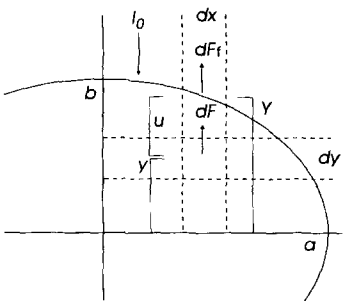

FIGURE 12. Geometry of internal filtering effects in a fiber of elliptic cross-section. Exciter light of intensity I_0 traverses a distance u inside fiber to reach a region $dydx$, where it elicits fluorescence of intensity dF. This light has to again traverse distance u to emerge as dF_f. See text for details.

The total fluorescence collected is the background, F_b, plus the integral of dF_f over the elliptical section. The integration over dy can be done analytically.

Let $Y = (b/a)\sqrt{(a^2 - x^2)}$. Then

$$\int_{-a}^{a}\int_{-Y}^{Y} dF_f(x,y) = \frac{q\ I_0\ D_1\ \epsilon_{1,\lambda}}{\ln 10\,(C_1 + C_2)} \int_{-a}^{a} \{1 - \exp[-2\ln 10\,(C_1 + C_2)\, Y(x)]\}\, dx =$$

$$\frac{q\ I_0\ D_1\ \epsilon_{1,\lambda}}{\ln 10\,(C_1 + C_2)}\ G(a,b,C_1,C_2) \tag{A4}$$

where G is a function that summarizes geometry and is calculated numerically.

This equation applies whether the fluorescent dye is free or bound to Ca^{2+}, although the parameters vary. When the fluorescent dye is free, q is at its minimum (q_{min}), and when bound, it is at its maximum. At the wavelengths used, $\lambda = 490$ and $\lambda_f = 530$ nm, q_{min} and q_{max} are at or near their highest values for fluo-3 and calcium green-1. The extinction coefficients of the two dyes at the two wavelengths (contained in C_1 and C_2) vary in general when the dyes bind Ca^{2+}; however, at the wavelengths 490 and 530 nm, both changes are ~10% (Harkins et al., 1993) and were neglected.

In general, the total fluorescence intensity will be

$$F([Ca^{2+}]) = \frac{F_b + (q_{min}\ D_1 + q_{max}\ D_1 Ca)\, I_0\ \epsilon_{1,\lambda}}{\ln 10\,(C_1 + C_2)} \tag{A5}$$

a function bounded by

$$F_{min} = F_b + \frac{q_{min}\, D_T\, I_0\, \epsilon_{1,\lambda}}{\ln 10\ (C_1 + C_2)} \tag{A6}$$

where D_T is total fluorescent dye concentration, and

$$F_{max} = F_b + \frac{q_{max}\, D_T\, I_0\, \epsilon_{1,\lambda}}{\ln 10\ (C_1 + C_2)}$$

F is a function of $[Ca^{2+}]$ through the functions D_1 and D_1Ca, which in equilibrium are

$$D_1 = \frac{D_T K_D}{Ca^{2+} + K_D}, \text{ and } D_1Ca = \frac{D_T Ca^{2+}}{Ca^{2+} + K_D}$$

Substituting in Eq. A5

$$F = \frac{F_{min} K_D + F_{max} Ca^{2+}}{Ca^{2+} + K_D} \quad (A7)$$

Eq. A7 yields the well known text Eq. 1. For the typical parameter values found in these experiments, the geometric factor G is very close to $0.75\ d\ \{1 - \exp[-\ln 10\ (C_1 + C_2)\ p]\}$, which is the expression that would apply to a body of rectangular cross-section of dimensions d and p, with a geometric correction factor of $\sim$0.75 that accounts for the lower area of the ellipse. Combining Eqs. A7 and A6, one gets text Eq. 5. Making $D_2 = 0$, text Eq. 2 is obtained. In the present paper, the exact expression Eq. A4 was used for G.

APPENDIX B

A Lattice Model of Ca^{2+}-dependent Activation

Fig. 11 illustrates an implementation, in the simplest quantitative terms, of a model of Ca^{2+}-dependent activation that uses the structural pattern of Block et al. (1988) and the dual control hypotheses of Ríos and Pizarro (1988). We considered a section of tubule constituted by a double row of alternating C and V channels, of currents i_C and i_V, situated at 30 nm between centers in a square array. The segment considered comprised 14 V and 14 C channels (the largest model size that could be handled by a PC computer's system memory). In a run with 12 channels, the results were qualitatively similar, suggesting that increasing the number of channels in the simulation would probably not generate new features. Each open V channel was assumed in the steady state to generate a profile of $[Ca^{2+}]$ (Fig. 11 *A*, *thick traces*) given by Stern's approximate Eq. 13 (Stern, 1992)

$$[Ca^{2+}] = [(Q_1 - Q_0) \exp(-r/\lambda) + Q_0]/r \quad (B1)$$

where r is the distance from the channel. Dr. Michael Stern (Johns Hopkins, Reisterstown, MD) kindly performed numerical calculations that showed the equation to be an adequate approximation in the conditions of our experiments. In particular, his calculations were for a 1 pA channel, in the presence of 1.5 mM of a diffusion limited buffer of K_D = 10 μM (to imitate our dyes plus intrinsic fast buffering) and 10 mM EGTA. These calculations also yielded values for the parameters Q_1, Q_0, and λ, which were used as initial guesses in our simulations.

When several V channels were open simultaneously, $[Ca^{2+}](x)$ was calculated by superposition of contributions evaluated with the same equation (thin trace in Fig. 11). The use of superposition was again shown by Stern to yield results within 25% of numerical calculations, at distances from the sources >30 nm. Since the channel current estimated from our present results was 0.15 (rather than 1) pA, 25% is probably an upper bound of the error caused by the use of superposition.

Although in the diagram (Fig. 11 *A*) $[Ca^{2+}]$ is represented as a function of the coordinate x, in the actual model the distances were calculated in the two dimensions of Fig. 11 *B*.

The calculated $[Ca^{2+}](x)$ was then compared with a threshold $[Ca^{2+}]$ (an adjustable parameter), to determine the state, open or closed, of every C channel in the group of 14. This calculation was carried out at every possible value of p_o, the open probability of V channels, that is, for 1, 2, . . . n_V, . . ., 14 V channels open. Shown in Fig. 11 *A* is one of the possible configurations with three channels open (of which there are 14!/(11!3!) different ones). For every configuration, the number of C channels open (n_C) was obtained, and then the ratio $(n_C i_C + n_V i_V)/n_V i_V$, which constitutes the *ratio* of peak over steady release predicted by the model for that particular configuration. This was repeated for all possible configurations of n_V open channels (14!/((14−n_V)!n_V!)), and the ratios were averaged. This average is the flux *ratio* predicted by the model at $p_o = n_V/14$. The different configurations of 14 V channels with n_V open were calculated with a FORTRAN routine (termed "spin-lattice," for it was written to solve an isomorphic problem of solid-state physics) kindly given and explained to us by Dr. Duanpin Chen (Rush University, Chicago, IL).

Using the experimental dependence of R_s with voltage (Fig. 7 *A*), and assuming that the maximum of R_s corresponds to p_o = 1, a representative experimental dependence p_o [V] was generated. The function *ratio* (p_o) given by the model was mapped to the voltage axis as *ratio* (p_o [V]) to give the function represented in Fig. 11 *B* by open symbols. The representation is for $i_C = i_V$, if i_C and i_V are different, the general scaling and limit values of the ratio change, but the qualitative features of the dependence stay the same.

The solid symbols were obtained by reducing the amplitude parameters (Q_1 and Q_0), which corresponds approximately to the effect of reducing the individual channel flux. As can be seen, the intermediate region of high ratio was reduced, but at the cost of introducing a region in which the ratio increases gradually with voltage. The model only has four adjustable parameters, the two Qs and λ in Eq. B1, and the threshold $[Ca^{2+}]$ for activation. Given this limited number, it was possible to explore a 10-fold range of values around

the starting point provided by Stern's calculations. It was not possible to reproduce even qualitatively the sharp increase with voltage, followed by a nearly constant ratio, observed for rat muscle.

We are grateful to Dr. Michael Stern, for extensive discussions, for calculations to verify the adequacy of, and find parameter values for Eq. 6, and for calculations to verify the adequacy of using superposition to estimate $[Ca^{2+}]$ resulting from the opening of multiple channels. We thank Dr. Duanpin Chen for showing us the isomorphism between finding open-close configurations of a set of channels and spins in a lattice, and for the routine used to generate those configurations. Drs. Elizabeth Stephenson and Clara Franzini-Armstrong provided illuminating insights, discussions, and access to unpublished data.

The work was supported by grants from the National Institutes of Health and MDA to E. Ríos, and NIH grants to Kurt Beam, to whom we are also indebted.

Original version received 13 March 1995 and accepted version received 15 May 1995.

REFERENCES

Airey, J. A., C. F. Beck, K. Murakami, S. J. Tanksley, T. J. Deerinck, M. H. Ellisman, and J. L. Sutko. 1990. Identification and localization of two triad junctional foot protein isoforms in mature avian fast twitch skeletal muscle. *J. Biol. Chem.* 265:14187–14194.

Anderson, K., A. H. Cohn, and G. Meissner. 1994. High affinity [^{3}H]PN200-110 and [^{3}H]Ryanodine binding to rabbit and frog skeletal muscle. *Am. J. Physiol.* 266:C462–C466.

Anderson, K., R. Grunwald, A. El-Hashem, R. Sealock, and G. Meissner. 1990. High affinity ryanodine and PN200-110 binding to rabbit skeletal muscle triads. *Biophys. J.* 57:171*a*. (Abstr.)

Baylor, S. M., W. K. Chandler, and M. W. Marshall. 1983. Sarcoplasmic reticulum calcium release in frog skeletal muscle fibers estimated from arsenazo III calcium transients. *J. Physiol.* 344:625–666.

Baylor, S. M., M. E. Quinta-Ferreira, and C. S. Hui. 1985. Isotropic components of Antipyrylazo III signals from frog skeletal muscle fibers. *In* Calcium in Biological Systems. R. P Rubin, G. Weiss, and J. W. Putney, Jr., editors. Plenum Publishing Corp., New York. 339–349.

Bers, D. M., and V. M. Stiffel. 1993. Ratio of ryanodine to dihydropyridine receptors in cardiac and skeletal muscle and implication for E-C coupling. *Am. J. Physiol.* 264:C1587–C1593.

Block, B. A., T. Imagawa, K. P. Campbell, and C. Franzini-Armstrong. 1988. Structural evidences for direct interaction between the molecular components of the transverse tubule/sarcoplasmic reticulum junction in skeletal muscle. *J. Cell. Biol.* 107:2587–2600.

Brum, G., E. Ríos, and E. Stefani. 1988. Effects of extracellular calcium on the calcium movements of excitation contraction coupling in skeletal muscle. (Appendix by G. Brum, E. Ríos, and M. F. Schneider) *J. Physiol.* 398:441–473.

Bull, R., and J. J. Marengo. 1993. Sarcoplasmic reticulum release channels from frog skeletal muscle display two types of calcium dependence. *FEBS (Fed. Eur. Biochem. Soc.) Letters.* 331:223–227.

Conti, A., P. Tarroni, D. Rossi, and V. Sorrentino. 1995. Ryanodine receptors: isoforms expression in mammals and chicken. *Biophys. J.* 68:A52 (Abstr.).

Delbono, O., and E. Stefani. 1993. Calcium transients in single mammalian skeletal muscle fibers. *J. Physiol.* 463:689–707.

Dulhunty, A. F., and C. Franzini-Armstrong. 1975. The relative contribution of the folds and caveolae to the surface membrane of frog skeletal muscle fibers at different sarcomere length. *J. Physiol.* 250:513–539.

Dulhunty, A. F., P. R. Junankar, and C. Stanhope. 1992. Extrajunctional ryanodine receptor in the terminal cisternae of mammalian skeletal muscle fibers. *Proc. R. Soc. Lond. B. Biol. Sci.* 247:69–75.

Eisenberg, B. R. 1983. Quantitative ultrastructure of mammalian skeletal muscle. *In* Handbook of Physiology, Skeletal Muscle. L. D. Peachey, R.-H. Adrian and S. R. Geiger, editors. American Physiological Society, Bethesda, MD. 3:73–112.

Francini, F., and E. Stefani. 1989. Decay of slow calcium current in twitch muscle fibers of the frog is influenced by intracellular EGTA. *J. Gen. Physiol.* 94:953–969.

Franzini-Armstrong, C. 1972. Studies of the triad. III. Structure of the junction in fast twitch fibers. *Tissue and Cell.* 4:469–478.

Franzini-Armstrong, C., and J. W. Kish. 1995. Alternate disposition of tetrads in peripheral couplings of skeletal muscle. *J. Muscle Res. Cell Motil.* 16:319–324.

García, J., and M. F. Schneider. 1993. Calcium transients and calcium release in rat fast-twitch skeletal muscle fibers. *J. Physiol. (Lond.).* 463:709–728.

García, J., and E. Stefani. 1990. Calcium transients in rat skeletal muscle: evidence for a Ca^{2+}-regulated Ca^{2+} release process. *Biophysiol. J.* 57:A400 (Abstr.).

González, A., and E. Ríos. 1993. Perchlorate enhances transmission in skeletal muscle excitation-contraction coupling. *J. Gen. Physiol.* 102:272–421.

Harkins, A. B., N. Kurebayashi, and S. M. Baylor. 1993. Resting myoplasmic free calcium in frog skeletal muscle fibers estimated with fluo-3. *Biophys. J.* 65:865–881.

Irving, M., J. Maylie, N. L. Sizto, and W. K. Chandler. 1987. Intrinsic optical and passive electrical properties of cut frog twitch fiber. *J. Gen. Physiol.* 89:1–41.

Jacquemond, V., L. Csernoch, M. Klein, and M. F. Schneider. 1991. Voltage-gated and calcium-gated calcium release during depolarization of skeletal muscle fibers. *Biophys. J.* 60:867–873.

Klein, M. G., B. J. Simon, G. Szucs, and M. F. Schneider. 1988. Simultaneous recording of calcium transients in skeletal muscle using high and low affinity calcium indicators. *Biophys. J.* 55:971–988.

Kovács, L., E. Ríos, and M. F. Schneider. 1983. Measurements and

modification of free calcium transients in frog skeletal muscle fibers by a metallochromic indicator dye. *J. Physiol. (Lond.).* 343: 161–196.

Lai, F. A., H. P. Erickson, E. Rousseau, Q.-Y. Liu, and G. Meissner. 1988. Purification and reconstruction of the calcium release channel from skeletal muscle. *Nature (Lond.).* 331:315–319.

Lai, F. A., Q. Y. Liu, L. Xu, A. El Hashem, N. R. Kramarcy, R. Sealock, and G. Meissner. 1992. Amphibian ryanodine receptor isoforms are related to those of mammalian skeletal or cardiac muscle. *Am. J. Physiol.* 263:C365–C372.

Lamb, G. D. 1992. DHP receptors and excitation-contraction coupling. *J. Muscle Res. Cell Motil.* 13:394–405.

Luff, A. R., and H. L. Atwood. 1971. Changes in the sarcoplasmic reticulum and transverse tubular system of fast and slow skeletal muscles of the mouse during postnatal development. *J. Cell Biol.* 51:369–383.

Margreth, A., E. Damiani, and G. Tobaldin. 1993. Ratio of dihydropyridine receptors in mammalian and frog twitch muscles in relation to the mechanical hypothesis of excitation-contraction coupling. *Biochem. Biophys. Res. Commun.* 197:1303–1311.

McKemy, D., A. Ivanenko, J. L. Kenyon, J. A. Airey, and J. L. Sutko. 1995. The αRyR influences the type of E-C coupling used in embryonic chicken skeletal muscle. *Biophys. J.* 68:A50. (Abstr.)

Melzer, W., E. Ríos, and M. F. Schneider. 1984. Time course of calcium release and removal in skeletal muscle fibers. *Biophys. J.* 45:637–641.

Melzer, W., E. Ríos, and M. F. Schneider. 1987. A general procedure for determining calcium release in frog skeletal muscle. *Biophys. J.* 51:849–864.

Murayama, T., and Y. Ogawa. 1992. Purification and characterization of two ryanodine binding isoforms from sarcoplasmic reticulum of bullfrog skeletal muscle. *J. Biochem.* 112:514–522.

O'Brien, J., G. Meissner, and B. A. Block. 1993. The fastest contracting muscles of nonmammalian vertebrates express only one isoform of the ryanodine receptor. *Biophys. J.* 65:2418–2427.

Ríos, E., and G. Pizarro. 1988. Voltage sensors and calcium channels of excitation-contraction coupling. *News Physiol. Sci.* 3:223–227.

Ríos, E., and G. Pizarro. 1991. Voltage sensor of excitation-contraction coupling in skeletal muscle. *Physiol. Rev.* 71:849–908.

Schneider, M. F., B. J. Simon, and G. Szucs. 1987. Depletion of calcium from sarcoplasmic reticulum during calcium release in frog skeletal muscle. *J. Physiol. (Lond.).* 392:167–192.

Shirokova, N., A. Gonzalez, J. Ma, R. Shirokov, and E. Ríos. 1995. Properties and roles of intramembranous change mobilized at high voltages in skeletal muscle. *J. Physiol. (Lond.).* 486:385–400.

Smith, J. S., T. Imagawa, J. J. Ma, M. Fill, K. P. Campbell, and R. Coronado. 1988. Purified ryanodine receptor from rabbit skeletal muscle is the calcium-release channel of sarcoplasmic reticulum. *J. Gen. Physiol.* 92:1–26.

Somlyo, A. V., H. Shuman, and A. P. Somlyo. 1977. Elemental distribution in striated muscle and the effect of hypertonicity: electron probe analysis of cryo sections. *J. Cell Biol.* 74:828–857.

Stern, M. D. 1992. Buffering of calcium in the vicinity of a channel pore. *Cell Calcium.* 13:183–192.

Takeshima, H., S. Nishimura, T. Matsumoto, H. Ishida, K. Kangawa, N. Minamino, H. Matsuo, M. Udea, T. Hanaoka, T. Hirose, and S. Numa. 1989. Primary structure and expression from complementary DNA of skeletal muscle ryanodine receptor. *Nature (Lond.).* 339:439–445.